Published in final edited form as:
Neuroscience. 2003 ; 121(1): 51–63.

IN VIVO BLOCKADE OF *N*-METHYL-D-ASPARTATE RECEPTORS INDUCES RAPID TRAFFICKING OF NR2B SUBUNITS AWAY FROM SYNAPSES AND OUT OF SPINES AND TERMINALS IN ADULT CORTEX

S. Fujisawa and **C. Aoki***
Center for Neural Science, New York University, 4 Washington Place, Room 809, New York, NY 10003, USA

Abstract

We investigated the role of *in vivo* synaptic activity upon trafficking of the *N*-methyl-D-aspartate (NMDA) receptor subunit, NR2B, at mature synapses by electron microscopic immunocytochemistry. *In vivo* blockade of NMDA receptors was achieved by applying the NMDA receptor antagonist, D-2-amino-5-phosphonovalerate (D-APV), onto the cortical surface of one hemisphere of anesthetized adult rats. Inactive L-2-amino-5-phosphonovalerate (L-APV) was applied to the contralateral hemisphere for within-animal control and to assess basal level of NR2B subunits at synapses. Within 30 min of D-APV treatment, we observed a decrease in the number of layer I axo-spinous asymmetric synapses that are positively immuno-labeled for the NR2B subunits. This decrease was paralleled by reductions in the absolute number of immuno-gold particles found at these synapses. The decrease of NR2B labeling was detectable in all five animals examined. Significant reductions were seen not only at post-synaptic densities, but also within the cytoplasm of spines and axon terminals. The data demonstrate that blockade of NMDA receptors induces trafficking of NR2B subunits out of synaptic membranes, spines, and terminals. This is in sharp contrast to a previous observation that NR2A subunits move into spines and axon terminals following *in vivo* blockade with D-APV. These findings point to yet unknown, NMDA receptor activity-dependent mechanisms that separately regulate the localization of NR2A and NR2B subunits at synapses.

Keywords

activity-dependent; D-APV; electron microscopy; immunocytochemistry; ultrastructure; post-embedding colloidal gold labeling

The *N*-methyl-D-aspartate (NMDA) subtype of glutamate receptor plays an important role in experience-dependent plasticity. Calcium influx through this receptor can trigger a variety of downstream biochemical reactions, contributing to plasticity (Mori and Mishina, 1995; Kind and Neumann, 2001) and excitotoxicity (Lynch and Guttmann, 2002). One of many consequences of NMDA receptor activation is altered trafficking of proteins to and from the activated synapses. For example, long-term potentiation, in which the electrophysiological response to an input is augmented, is in part produced by NMDA receptor-dependent up-regulation of synaptic α-amino-3-hydroxy-5-methyl-4-isoxazolepropionic acid receptors (see

*Corresponding author. Tel: +1-212-998-3929; fax: +1-212-995-4011. chiye@cns.nyu.edu (C. Aoki).

review Malenka and Nicoll, 1999). *In vitro* and fewer *in vivo* preparations have been used to demonstrate that NMDA receptors, too, are removed from or inserted into synaptic membrane (Rao and Craig, 1997; Liao et al., 1999; Quinlan et al., 1999; Heynen et al., 2000; Barria and Malinow, 2002; Grosshans et al., 2002; Tovar and Westbrook, 2002). However, since nearly all of these studies have used neonatal tissues, whether or not such dynamic properties of NMDA receptor subunits persist at mature synapses, *in vivo*, is a topic that remains relatively unexplored.

Among the NMDA receptor subunits, the NR1 is necessary for NMDA receptor function, but the NR2 subunits may be relatively more central in determining NMDA receptor localization (Mori et al., 1998; Steigerwald et al., 2000; Mohrmann et al., 2002) because their C-termini are longer and permit interaction with postsynaptic density (PSD) scaffolding proteins, such as PSD-95 (Niethammer et al., 1996; Bassand et al., 1999; Sheng and Pak, 2000). Among the NR2 subunits, the NR2A and NR2B subtypes are the most prevalent in the cerebral cortex (Watanabe et al., 1992), and of the two, the NR2B subunits are shown to be particularly influential in learning and memory (Tang et al., 1999; Tang and Schuman, 2002) as they prolong NMDA receptor currents, thus allowing greater Ca influx (Mori and Mishina, 1995; Dingledine et al., 1999). Further, Roche et al. (2001) have shown that the C-terminus of NR2B subunit is sufficient for rapid internalization of the NMDA receptor.

The present study focused on activity-dependent trafficking of endogenous NR2B subunits in adult rat cortex. We applied a competitive NMDA receptor antagonist, D-2-amino-5-phosphonovalerate (D-APV), onto one hemisphere of intact anesthetized, adult rat cortices. For each animal, the contralateral hemisphere served as a control and was treated with inactive L-APV. Inter-hemispheric differences in the presence of NR2B subunits at presynaptic, postsynaptic, and non-synaptic sites were detected using colloidal gold as the label for electron-microscopic immunocytochemistry (EM-ICC).

EXPERIMENTAL PROCEDURES

Surgery and drug treatment

NMDA receptor activity at intact mature synapses of adult cortices was blocked by topical application of an NMDA receptor antagonist, D-APV, over the cortex while maintaining the animal anesthetized. Six adult Sprague–Dawley rats (#9, #10, #11, #12, #52699-1, #52699-2; five males and one female), weighing 220 g–390 g were used (Hilltop, PA, USA). All rats were anesthetized with Nembutal (Abbott Laboratories, IL, USA; 25 mg/kg; i.p.). For rats #9–#12, the anesthesia was followed by an injection of atropine (Elkins-Sinn, Inc., NJ, USA; 0.08 mg/kg; intramuscular) to minimize respiratory complications. A stereotaxic apparatus was used to stabilize the animal's head during neurosurgery. Once the skull was exposed and cleaned, relatively large holes (1 mm radius) were drilled at the following stereotaxic coordinates, AP: −1 mm, ML: ±2 mm, targeting the somatosensory cortex. The exposed dura mater was punctured using a 26-gauge needle tip. A small piece of sterile gel foam (approximately 1 mm×3mm) was saturated with 5 mM D-APV (Sigma, OR). The solvent was artificial cerebrospinal fluid (115 mM NaCl, 3.3 mM KCl, 1 mM $MgSO_4$, 2 mM $CaCl_2$, 25.5 mM $NaHCO_3$, 1.2 mM NaH_2PO_4, 5 mM lactic acid, and 25 mM glucose, equilibrated with 95% O_2−5% CO_2) for animals #9–#12 and sterile saline (B. Braun Med Inc., CA, USA) for animals #52699-1 and #52699-2. The drug-soaked gel foam (Pharmacia & Upjohn Co., MI, USA) was placed directly over the punctured dura. For animals #9–#12, the contralateral cortex was treated identically, but with the inactive enantiomer, L-APV (Sigma Chem, OR, USA). The control hemispheres of animals #52699-1 and #52699-2 received sterile saline alone. The hemisphere treated with D-APV was counterbalanced across the animals. The drug application lasted for 30 min for animals #9–#12, 1 h for #52699-1, and 2 h for #52699-2. These methodological details are summarized in Table 1. One animal, #10, suffered respiratory arrest

during the surgery, and was not included in tissue processing or data analysis. The drug application period was terminated by perfusing the animals transcardially first with heparinized saline (heparin; ESI Pharmaceuticals, NY, USA), then with a fixative consisting of 4% paraformaldehyde mixed with 1% glutaraldehyde (Electron Microscopic Sciences, PA, USA). All other chemicals listed here and in other sections of the Procedure were purchased from Sigma Chem (OR, USA) unless otherwise noted. All surgical procedures were in accordance with the National Institutes of Health Guide for the Care and Use of Experimental Animals and were approved by the NYU Animal Care and Use Committee. Consideration was made in the experimental design to minimize discomfort or suffering to the animals and of the number used.

Preparation of tissue for ICC detection of NR2B subunits

The brain was dissected out of the skull. The region underlying the drilled skull and duratomy was first cut into 3–4 mm coronal blocks with a razor blade. Then the ventral portion of the left hemisphere was cut off to mark the left side. The blocks were cut into 40 μm-thick coronal sections using a vibratome. Aldehyde-fixation was terminated with 1% sodium borohydride in 0.1 M phosphate buffer (PB), pH 7.4. After rinsing in PB, the free-floating sections were stored at 4 °C in a buffer consisting of 0.01 M PB with 0.9% sodium chloride and 0.05% sodium azide.

In preparation for immunogold labeling, the vibratome sections underwent osmium-free processing (Phend et al., 1995; Aoki et al., 2001) to preserve both antigenicity and ultrastructure. The vibratome sections were incubated in a series of solutions interleaved by washes in 0.1 M maleate buffer (pH 6.0). All solutions were dissolved in maleate buffer, and the procedures were done on ice. The incubations were 40 min in 1% tannic acid (EM Sciences, PA, USA), 40 min in 1% uranyl acetate (EM Sciences, PA, USA), then 20 min in 0.5% iridium tetrabromide (Alfa Aesar, MA, USA). Still on ice, the sections were washed in 50% ethanol and then 70% ethanol. They were incubated for 2 days at 4 °C in 1% uranyl acetate dissolved in 70% ethanol. Then at room temperature, the sections were dehydrated sequentially in 70%, 90% and 100% ethanol and then in 100% acetone. The sections from animals #9-#12 were infiltrated with Epon (EM Sciences, PA, USA), while those from the other animals were incubated in Epon-Spurr (EM Sciences, PA, USA) overnight (see Table 1). The treated brain area for each animal was capsule-embedded in Epon or Epon-Spurr, flat embedded and then ultra-thin sectioned at a thickness of approximately 80 nm. The ultra-thin sections spanned the supragranular and granular layers of cortex.

Immunocytochemical detection of NR2B by the post-embedding colloidal gold labeling (PEG) procedure

To minimize experimental errors, the grids with tissues from the D-APV treated and control regions were immuno-labeled simultaneously. All incubations were performed at room temperature. Formvar-coated grids holding the ultra-thin sections were rinsed in 0.05 M Tris buffer containing 0.9% NaCl and 0.1% Triton X-100 (TBST, pH 7.4). The grids were then incubated overnight in droplets containing the primary antibody, rabbit anti-NR2B-antiserum (Upstate, NY, USA), prepared at a concentration of 10 μg/ml using TBST at pH 7.4. After rinsing in TBST (pH 7.4), the grids were then incubated for 3 h in goat anti-rabbit IgG antibody conjugated to 15 nm colloidal gold particles (Ted Pella, Inc.; Redding, CA, USA). This secondary antibody was diluted 1:40 using TBST, pH 8.2. The ultra-thin sections were post-fixed for 15 min using 1% glutaraldehyde. The grids were counter-stained with Reynold's lead citrate (EM Sciences, PA, USA) for 20 s. After drying, the grids were examined under the electron microscope (EM; JEOL 1200XL, Tokyo, Japan).

Data sampling

Rationale for sampling synapses from layer I—Initially, we sampled 50 synapses from each of layers I and II/III in both the control and experimental hemispheres of animal #9. Analysis of these synapses (described in detail below) revealed that in layer I, there were hemispheric differences in the amount of immunolabeling at synapses. In contrast, synaptic labeling in layer II/III of the D-APV-treated region was not significantly different from that in the contralateral control neuropil, suggesting that D-APV solution might not have diffused into layer II/III within 30 min. For all animals thereafter, data were collected exclusively from layer I.

Identification of sampling area in layer I—Layer I was easily identifiable as the synaptic neuropil underneath the pial surface that is devoid of neuronal cell bodies or apical dendrites. Pia mater was recognized by its smooth, continuous glial lining and its juxtaposition to embedding material. The presence of large neuronal somata denoted the upper limit of layer II. We examined the immunolabeling in regions of layer I that departed from pia by at least 5 μm. Tissue near the punctured dura mater showed swollen mitochondria. We avoided these regions, but otherwise stayed as close as possible to the duratomy site. Images of this sampling area were digitally or photographically captured at a magnification of 25,000×.

Criteria used to identify asymmetric synapses—Using the captured micrographs at 25,000× magnification, 100 asymmetric axo-spinous synapses were counted in each hemisphere of each animal. Asymmetric synapses were presumed to be excitatory, and thus glutamatergic (DeFelipe et al., 1988; Aoki et al., 1994; Kharazia and Weinberg, 1999). An asymmetric synapse was identified as such using the following criteria: presence of parallel-aligned plasma membranes, denoting the synaptic cleft; the presence of vesicles, indicating that the juxtaposed profile was presynaptic; and the presence of electron-densities without vesicles, denoting the postsynaptic membrane. Whenever PSDs and vesicles could be identified together, visualization of the cleft was deemed unnecessary for identification of synapses.

Synaptic sampling procedure—Layer I neuropil was sampled by making systematic sweeps within the squared area bordered by the thin bars of the grids. In this way, 10 groups of 10 synapses were sampled in the order of appearance. This procedure was followed to assure unbiased sampling for statistical analyses and for detecting any trend in immunolabeling that varied as a function of distance from duratomy site. Synapse and subsequent gold-particle counts were conducted in a blinded manner.

Data analysis

Quantification of synapse density—We assessed whether D-APV treatment caused changes in synapse density. To this end, we used all micrographs collected for analysis of synaptic NR2B immunolabeling. Each micrograph captured 26.60 μm of layer I neuropil. Approximately 20 micrographs were available from each analyzed hemisphere. Using this set, we determined synapse density within experimental and control hemispheres by counting the number of synapses found in each micrograph. From these counts, we calculated the mean value of synapses per unit area, with the unit area set to 26.60 μm.

Quantification of NR2B labeling, using synapses as the unit for counting—We wanted to examine primarily the changes in the distribution of synaptic NR2B subunits due to treatment with D-APV. The active zone of a synapse could be subdivided into three mutually exclusive areas: presynaptic membrane, synaptic cleft, and PSD. However, the pool of 100 synapses contained some that were “tilted” with no visible synaptic cleft. In such synapse, the gold particles at PSD and at presynaptic membrane cannot be clearly discriminated. Therefore, a synapse with immunolabeling at the active zone was categorized as a synapse labeled

anywhere "within pre- and postsynaptic area" (Fig. 1A). Separately, we also recounted the number of synapses with one or more gold particle anywhere "within terminals" but away from synapses, anywhere "near PSDs" but not at PSDs, anywhere "within spines" but away from synapses, and finally anywhere "within total synaptic area" (Fig. 1A). "Near" was defined as residing within the width equivalent to the thickness of one PSD. One synapse could be counted several times if it contained gold particles in more than one of these areas. Thus, for each group of 10 synapses, the maximum possible count within each category was 10.

Consequently, we wanted to separately analyze pre- and postsynaptic sides. In light of that, we eliminated the "tilted" synapses from the pool, in which the synaptic clefts were not clearly discernable. For these "non-tilted" synapses, we could determine the specific position of synaptic gold particles: "at/near presynaptic membranes," "at clefts" or "at PSDs" (see Fig. 1B). At least five groups of 10 synapses were obtained from each hemisphere. Synapses were counted into one or more of the following categories according to the position of immunogold particles with respect to the synaptic cleft. The mutually exclusive categories were (see Fig. 1B): synapses labeled anywhere "within terminals," "at/near the presynaptic membranes," "at clefts," "at PSDs," "near PSDs," and anywhere "within spines." Progressively inclusive categories were as follows: "within postsynaptic area" included synapses with one or more gold "at clefts" or "at PSDs"; "within pre- and postsynaptic area" included synapses with one or more gold "at clefts," "at PSDs," or "at/near presynaptic membranes"; lastly "within total synaptic area" included synapses with one or more gold anywhere within the profile.

Quantification of NR2B labeling, using gold particles as the unit for counting— Furthermore, we counted the absolute number of gold particles found for every group of 10 synapses (n = 10 for each hemisphere of each animal). The particles found in each of the following regions were counted separately (see Fig. 1A): "within terminals," "within pre- and postsynaptic area," "near PSDs," and "within spines." In addition, all gold particles found within the synaptic profile were tallied together in an inclusive category, "within total synaptic area."

For the select pool of "non-tilted" synapses only, the gold particles were categorized according to more specific positions (see Fig. 1B). We used the same mutually exclusive categories as we did for labeled synapse counts: "within terminals," "at/near presynaptic membranes," "at clefts," "at PSDs," "near PSDs," and "within spines." The inclusive category of "within postsynaptic area" was calculated as the sum of gold counts in the "at cleft" and "at PSD" categories. The values in the "within pre- and postsynaptic area" category were calculated by taking the sum of gold counts in the "postsynaptic" and "at/near presynaptic membranes" categories. "Within total synaptic area" category represented all gold particles found in all areas of the synaptic profile.

Statistical analysis of the intra-animal difference in synaptic NR2B immunolabeling—In all analyses, average number of synapse or gold counts for every group of 10 synapses, and their S.E.M., were calculated. In order to determine the significance of D-APV-induced changes in synaptic NR2B distribution, we used a two-tailed Student's t-test assuming unequal variances, identifying within-animal interhemispheric differences. The significance level was set at $P<0.05$.

Analysis of synaptic and non-synaptic NR2B labeling—A subset of micrographs used for NR2B labeling analysis was also used to assess whether the D-APV application caused changes in the overall antigenicity of NR2B subunits. The minimum number of micrographs used was nine per hemisphere per animal. All gold particles, present anywhere in the neuropil, were counted, and the average number of particles per unit area (26.60 μm) was calculated for

treated and control neuropil. The two-tailed Student's *t*-test' was used to assess significance of differences.

RESULTS

Minimal ultrastructural changes induced by D-APV infusion

The cortex beneath the craniotomy site was indented slightly. The dents were present on both experimental and control hemispheres. Light microscopic inspection of Nissl-stained sections of these regions showed compressed cell bodies but there were no noticeably unhealthy cells, blood clots, or tissue tearing. Using the EM, at a magnification of 25,000×, we observed zones of neuropil containing swollen dendrites and mitochondria immediately adjacent to the duratomy site (ca 100 μm). We collected data from regions that were as close as possible to the duratomy site and yet free of such signatures of metabolic stress.

In four out of five animals analyzed, the total area of layer I required to encounter 100 synapses was slightly less for the D-APV-treated region, indicating a slight increase in the areal density of synapses (Fig. 2). In only one animal (#52699-2) was this difference statistically significant (two-tailed *t*-test, $P<0.05$). For quantification of changes in NR2B labeling, analyses were normalized to the number of synapses encountered rather than the area surveyed, so that the measurement would be independent of spine density changes.

Analysis of NR2B immunolabeling in layer I

All detailed counts and analysis of NR2B immunolabeling was conducted within layer I. It has been shown that layer I contains more synapses with NMDA receptors than deeper layers (Aoki et al., 1994); therefore, we predicted that a great amount of synapses would be affected by the D-APV application in this layer. Earlier published work (Aoki et al., 2003) showed that, indeed, the effect of D-APV upon NR2A subunits is restricted to layer I during the first 2 h of surface application of the drug. Pilot studies revealed that D-APV-induced changes in NR2B distribution also were restricted to the upper-most layer (Figs. 2, 4 and 5). We interpret this result as the inability of D-APV to diffuse into deeper layers within the treatment duration (30–120 min.). Due to the high concentration of NMDA-receptor containing profiles in layer I, it is possible that synapses in this layer are highly responsive to D-APV application when compared with synapses in other layers.

Immuno-gold NR2B labeling was present at synapses, as well as within the cytoplasm of postsynaptic spine and presynaptic terminal. Fig. 3 contains examples of representative synapses that we encountered.

Within a region deemed suitable for analysis, systematic sweeps of the neuropil were made under the EM. From each hemisphere of all five animals, 10 groups of 10 synapses (total of 100 synapses) from Layer I were analyzed in the order encountered so as to maintain unbiased sampling.

Reduction in the number of NR2B immuno-labeled synapses

For each group of 10 synapses, we allocated the synapses into one or more of following categories (Fig. 1a): having one or more gold particles anywhere "within terminals," "near PSDs," "within spines," "within pre- and postsynaptic area," and also having one or more particles anywhere "within total synaptic area" (Table 2). For all of the animals analyzed ($n=5$), the D-APV treated hemisphere showed less synaptic profiles with gold particles when compared with the L-APV treated side (Fig. 4; column E in Table 2). In three animals, the difference reached statistical significance (two-tailed *t*-test; $P<0.05$).

Similar reduction was seen in the number of synapses with gold particles "within pre- and postsynaptic area" (column D in Table 2). These results show that D-APV application induced a decrease in NR2B immunolabeling at and surrounding the synaptic cleft. Robust reduction was also seen in the number of synapses with gold particles "within terminals" and "within spines" but clearly removed from the active zone (columns A and C in Table 2 respectively). The smallest change in the NR2B labeling occurred near PSDs (column B in Table 2). This analysis showed that D-APV treatment induces a reduction in NR2B-subunit labeling in most areas of the synaptic profile. A substantial portion of synapses were no longer immunoreactive for NR2B subunits, even when tallied using the most inclusive criterion: one gold particle at or near the synapse (Fig. 4, column E in Table 2).

Reduction in the number of synaptic immuno-gold particles

The absolute number of gold particles found within the synaptic profile was recorded for each of 100 synapses (Table 3). The categories were the same as those for synapse count: "within terminals," "near PSDs," "within spines," "within pre- and postsynaptic area," and finally 'within total synaptic area,' which is a sum of all gold particles within the synaptic profile (Fig. 1A). This procedure of quantification again revealed a marked reduction of NR2B immunolabeling following D-APV treatment (Fig. 5; also column E in Table 3). Three out of five animals showed a statistically significant overall decrease associated with D-APV treatment (Fig. 5), and the *P*-value for the other animal (#11) was 0.066.

Less but consistent reduction was seen in the number of gold particles "within pre- and postsynaptic area" (column D in Table 3). The trend is also very clear "within terminals" and "within spines" (columns A and C in Table 3). As with synaptic counts, the results showed that there is an overall reduction in immunolabeling not just in the active zones but also within cytoplasm of spine heads and axon terminals.

Analysis of immuno-labeled "non-tilted" synapses

The pool of 100 synapses analyzed above included those that were sectioned at an angle not orthogonal to the plane of the cleft; i.e. "tilted." As a result, their synaptic clefts were not clearly visible. Analysis above revealed that there is strong reduction in immunolabeling residing at synapse. In order to discriminate changes in the presynaptic versus postsynaptic sides of the cleft, we further analyzed a subset of synapses for which the synaptic clefts were clearly visible. From this select pool, immunolabeling could be grouped into more specific categories (Fig. 1B). This way, we could determine if the reduction in NR2B labeling occurred presynaptically, postsynaptically, or both. The number of labeled synapse and gold particles were counted and analyzed again in this new group of synapses.

Immuno-labeled synapses were counted as belonging to one of the following six mutually exclusive categories, distinguished by the position of the colloidal gold (Fig. 1B): "within terminals" but away from synapse, "at/near presynaptic membrane," "at clefts," "at PSDs," "near PSDs," and "within spines" but away from synapse. In addition, tallying was done using three progressively inclusive categories (Fig. 1b): synapses with labeling anywhere "within postsynaptic area," anywhere "within pre- and postsynaptic area" and finally anywhere "within total synaptic area."

Fig. 3 shows examples of the mutually exclusive counting categories. The bottom synapse in panel A had gold particles within the terminal, within the spine, and at the PSD. Such a synapse would be tallied in three of the six mutually exclusive categories, i.e. "within terminals," "within spines," "at PSDs," and also in all three of the inclusive categories. In this manner, we tallied the number of these labeled "non-tilted" synapses (Table 4).

Strong reductions were seen postsynaptically (column G in Table 4). Although in only one animal (#12) were the differences significant, there was a consistent decrease across animals in the number of synapses immuno-labeled “at clefts” and “at PSDs” (columns C and D in Table 4). The reduction of synapses labeled “at/near presynaptic membranes” occurred to a lesser degree (column B in Table 4). When presynaptic and postsynaptic changes were pooled together, however, the reduction was very robust, with three animals reaching statistical significance (column H in Table 4).

Analysis of immuno-gold particles in “non-tilted” synapses

Gold count and analysis were also conducted in the pool of “non-tilted” synapses (Table 5). The mutually exclusive categories were the same was ones used in the synapse counts. The progressively inclusive categories were calculated as the sum of gold particles present in corresponding areas of the synaptic profile (Fig. 1B).

When analyzing with gold particles as the unit for counting, we saw stronger reduction presynaptically than postsynaptically. In two animals (#12 and #52699-1), there was significant decrease in gold particles “at/near presynaptic membrane” (column B in Table 5). The reduction of gold counts “at clefts” and “at PSDs” were modest, but it was very consistent across animals (columns C and D in Table 5).

Combined outcomes of all analyses indicate that D-APV treatment induced strong and consistent reduction in the NR2B immunolabeling at pre- and postsynaptic active zones of synapses as well as in the cytoplasm of spines and terminals.

Variability among animals

We observed great variability among animals. For animal #12, the decreases were significant both in the number of immuno-positive synapses and in the number of gold particles under most of the categories (Tables 2–5). On the other hand, for animal #11, there were small, insignificant reductions in all of the subcategories. In some animals, NMDA receptor blockade caused an increase in the level of NR2B labeling, but these changes were statistically insignificant (for example, categories “at/near presynaptic membranes” and “at PSDs” of animal #11, columns B and D in Tables 4 and 5). Although inter-animal variability was prominent, the most consistent result overall was that D-APV treatment caused reductions in synaptic subunit labeling for NR2B subunits.

Changes in overall immunoreactivity for NR2B subunits

To see if reduction in synaptic NR2B labeling was due to reduction in overall immunoreactivity for NR2B subunit after D-APV treatment, we quantified immuno-gold density over the entire neuropil without differentiating synaptic from non-synaptic regions following the standard PEG procedure. Hemispheric comparison of these data revealed that there were differences in total immunoreactivity between the D-APV treated and control regions. However, in contrast to the synaptic immunoreactivity, the inter-hemispheric difference in total immunoreactivity was much more variable, for some increasing, while for others decreasing within the D-APV treated neuropil (see Fig. 6). This outcome indicated that labeling at non-synaptic portions of neuropil followed a mechanism distinct from that regulating synaptic NR2B localization.

Background immunolabeling

The immunoreactivity for NR2B is relatively low, averaging at about 2.3 gold particles per synapse in the control neuropil. We determined the degree of non-specific labeling by analyzing the grids in which the primary antibody was eliminated from the PEG protocol. In the absence of the primary antibody, the density of colloidal gold was low, averaging 5.2 particles per

micrograph, spanning 26.60 μm of neuropil, and containing approximately five synapses. None of these gold particles were located over synapses.

DISCUSSION

NR2B subunits occur both pre- and post-synaptically

Colloidal gold particles allow relatively precise localization of the antigen (Fig. 3). Gold label occurred postsynaptically, directly over, or near the PSD complex and also within the cytoplasm of dendritic spines. These locations agree with results from past ultrastructural studies (Aoki et al., 1994;Charton et al., 1999;Conti et al., 1999;Kharazia and Weinberg, 1999;Valtschanoff and Weinberg, 2001). In addition, NR2B subunit labeling was prominent in the cytoplasm and along membranes of presynaptic terminals. This observation is also not unexpected, since NR2A and NR2B subunits have been seen presynaptically (Charton et al., 1999;Conti et al., 1999;Valtschanoff and Weinberg, 2001). Moreover, electrophysiological studies have shown that these presynaptic receptors function as autoreceptors, facilitating glutamate release (Berretta and Jones, 1996;Woodhall et al., 2001).

D-APV causes trafficking of NR2B subunits away from synapses

The present study showed that 30 min of NMDA receptor blockade induces a reduction in the synaptic labeling of NR2B subunit in adult rat cortex. This reduction was most consistent at synaptic portions of neurons. Our interpretation of the reduced synaptic immunoreactivity is that the NMDA receptor blockade causes net trafficking of NR2B subunits away from the active zone of synapses and also out of spines and terminals. NR2B subunits are known to be rapidly internalized in immature neurons (Roche et al., 2001). Activity-dependent trafficking of synaptic NR2B-containing receptors has been shown anatomically using *in vitro* fluorescent preparations (Rao and Craig, 1997), electrophysiologically (Tovar and Westbrook, 2002), and biochemically (Grosshans et al., 2002). While none of these methods or our EM-ICC have examined single synapse over time, a decrease consistent across a large population of synapses supports the idea that there is a mechanism for NR2B subunits to be trafficked out of the D-APV treated synapses. It is likely that these receptors are endocytosed in clathrin-coated vesicles (Roche et al., 2001; Carroll and Zukin, 2002). We did not encounter any NR2B-labeling gold particle associated with a pit. However, it is likely that internalization occurs so rapidly that it is rarely captured by electron microscopy.

Could D-APV treatment cause an overall reduction in the subunit's antigenicity? The aldehyde-conjugated drug could potentially interact with the antibodies, since the D-APV binding site (Nakanishi, 1992; Mori and Mishina, 1995) resides near the antigenic site (Sheng et al., 1994). However, there are several reasons why we think this interpretation is unlikely. The immunoreactive and non-immunoreactive synaptic junctions were found within few microns of one another: it is unlikely that synapses so close to one another would have had different exposures to D-APV. Such differences in immunoreactivity across synapses are more likely to arise from differences in the concentration of NR2B subunits. Second, the overall immunoreactivity of the drug-treated and control neuropil was assessed by counting the number of immunogold particles per unit area (Fig. 6). This analysis showed that in some animals, D-APV treated neuropil showed greater overall immunoreactivity while synaptic labeling still decreased.

An alternate explanation for the reduced NR2B immunolabeling is that the NR2B subunits were degraded instead of being trafficked out of spines or terminals. This remains a possibility. If so, receptors may be proteolyzed while still in the synaptic membrane or else are proteolyzed while being trafficked away from plasma membrane into the cytoplasm. Whether or not rapid

degradation of NR2B subunits is activity-dependent is an interesting subject that can be addressed in future studies using biochemical approaches.

NR2B subunit trafficking occurs quickly

Our D-APV treatment was brief (ca. 30 min) compared with other experiments studying the effects of D-APV on the trafficking of NMDA receptor subunits. These results suggest that trafficking of NR2B subunits out of spines and terminals is rather fast, allowing for the concentration of synaptic NR2B subunits to become altered within minutes following changes in synaptic activity.

After being trafficked out of spines terminals, where might the NR2B subunits go? One prediction is that a decline of synaptic labeling would be accompanied by a rise of immunoreactivity within non-synaptic portions of axons and dendrites. In order to test this hypothesis, one would need to measure the immunoreactivity within dendritic shafts and axons contiguous with the synapse showing NR2B reduction. Studies are under way to examine whether a decrease in the amount of NR2B subunits within layer I spines might be accompanied by elevations of NR2B subunits in other dendritic locations of the same population of neurons.

NR2B and NR2A subunits are regulated differently

Changes in the distribution of NR2B subunits, seen in this study, are in sharp contrast to the regulation of NR2A subunits. Our laboratory has previously shown that 30–120 min of NMDA receptor blockade by D-APV causes a significant increase in the number of NR2A subunits at synaptic sites as well as in spines and terminals (Aoki et al., 2003). The difference in the outcome of the two studies suggests lack of cross-reactivity of the NR2B and NR2A antibodies. More significantly, these results suggest that reduced activity of NMDA receptors may shift the overall distribution of NMDA receptor subunits, favoring greater localization of NR2A and less of NR2B subunits at synapses. This may cause subtle changes in the physiological properties of glutamatergic transmission. NR2B-containing receptors have slower receptor kinetics compared with NR2A-containing receptors (Mori and Mishina, 1995; Dingledine et al., 1999; Yamakura and Shimoji, 1999). Our findings predict that 30–120 min of NMDA receptor blockade could cause increases of NR2A-containing receptors, resulting in overall shortening of NMDA receptor current. Electrophysiological studies are needed to clarify whether sensitivity to ifenprodil, the antagonist selective for heteromers containing NR2B subunits, decreases after 30 min of NMDA receptor blockade by D-APV.

There are studies, besides ours, showing that NR2A and NR2B subunits are regulated differently (Williams et al., 1998; Quinlan et al., 1999; Barria and Malinow, 2002). How might this subunit-specific trafficking be achieved? The anchoring protein, PSD-95, binds to the PDZ-binding domain that is common to all NR2 subunits (Niethammer et al., 1996; Sheng, 2001). One possible mechanism for trafficking the NR2A- and NR2B-containing NMDA receptors in opposite directions is that PSD-95 responds to NMDA receptor blockade with intramolecular structural changes, leading to an increased affinity of PSD-95 for the NR2A subunits and decreased affinity for the NR2B subunits. Carroll and Zukin (2002) propose that phosphorylation of NR2B subunits by PKC disrupts its association with PSD-95, leading to its internalization. At the same time, Lan et al. (2001a) showed that activating PKC results in insertion of NR1-NR2A receptors. This phosphorylation step may have been enhanced by D-APV blockade of NMDA receptors. Furthermore, others have shown that metabotropic glutamate receptor activation results in trafficking of NR2 subunits (Lan et al., 2001b). Since D-APV does not prevent endogenous glutamate to bind to metabotropic glutamate receptors, this receptor may be involved in the phosphorylation-dependent switching of subunits from NR2B to NR2A subunits at synapses. It will be interesting to learn whether levels of phosphorylated NR2A and NR2B subunits following blockade of NMDA receptors are altered.

The experiments reported here are the first to visualize activity-dependent NMDA receptor regulation at an ultra-structural level of resolution, following short-term *in vivo* blockade of NMDA receptors in the adult sensory cortex. Only a few other studies have examined trafficking of NR2B subunits following NMDA receptor blockade of varying durations. Both Tovar and Westbrook (2002) and Rao and Craig (1997) demonstrated that inactivation of NMDA receptors results in an elevation of NMDA receptors at synapses, with no preference between NR2A- and NR2B-containing receptors. On the other hand, Barria and Malinow (2002) showed that while NR2A subunits are trafficked into the spine after D-APV treatment, NR2B subunits are not affected by it. The outcome of our study differs from theirs, in that we observe different directions of trafficking between NR2A and NR2B subunits. These differences may be as ascribable to our *in vivo* versus their *in vitro* preparations. Moreover, since they examined young hippocampal synapses in slice or culture while we studied mature cortical synapses, the set of proteins and mechanisms mediating receptor trafficking may be different. Yet another difference between their studies and ours is that the NMDA receptor blockade was greater than 24 h for theirs, but much shorter for ours. As the presence of D-APV is prolonged, secondary mechanism may start to take effect that reverse the effect we observed during the first 2 h.

Note that the decrease in immunoreactivity for NR2B subunits seen in our study was small and confined to spines and terminals. In our hands, these localized changes were not detectable by light microscopy. It is not surprising that our results differ from the above mentioned and other physiological findings that may have overlooked the changes in silent synapses (e.g. see ref Quinlan et al., 1999) or the biochemical measurements that, like our light microscopic analyses, examines changes that are averaged over larger volumes (Rao and Craig, 1997; Williams et al., 1998; Grosshans et al., 2002).

In conclusion, the combination of using an *in vivo* adult model, a pharmacological treatment confined to layer 1, and the precision afforded by EM makes this study unique. Although the pharmacological blockade of synaptic NMDA receptors by D-APV is hardly physiological, the responses evoked by this treatment reveals a rapid subcellular mechanism that can be recruited in response to varying degrees of synaptic activity. Specifically, our results from probing the NR2A and NR2B subunits predict that decreased synaptic activity, accompanied by decreased activation of NMDARs, leads to increases in temporal and spatial fidelity of NMDAR currents. In the future, we plan to determine whether local application of D-APV affects synapses in layer I only, or may activate intracellular mechanisms that influence other synapses of the same neuron residing in layers beyond reach of extracellularly applied D-APV.

Abbreviations

D(L)-APV	D(L)-2-amino-5-phosphonovalerate
EM	electron microscope
EM-ICC	electron microscopic immunocytochemistry
NMDA	*N*-methyl-D-aspartate
PB	phosphate buffer
PEG	post-embedding colloidal gold labeling
PSD	postsynaptic density
TBST	Tris-buffered saline containing Triton X-100

Acknowledgments

We thank Anita Disney and Robert Levy for their critical reading of the manuscript. This research was supported by R01-EY13145 and R01-NS 41091 to CA, the NEI Core Grant (1 P30 EY13079, PI-JA Movshon) and the Office of Naval Research Grant (BAA 99-019, PI-P Lennie).

REFERENCES

Aoki C, Fujisawa S, Mahadomrongkul V, Shah PJ, Nader K, Erisir A. NMDA receptor blockade in intact adult cortex increases trafficking of NR2A subunits into spines, postsynaptic densities, and axon terminals. Brain Res 2003;963:139–149. [PubMed: 12560119]

Aoki C, Miko I, Oviedo H, Mikeladze-Dvali T, Alexandre L, Sweeney N, Bredt DS. Electron microscopic immunocytochemical detection of PSD-95, PSD-93, SAP-102, and SAP-97 at postsynaptic, presynaptic, and nonsynaptic sites of adult and neonatal rat visual cortex. Synapse 2001;40:239–257. [PubMed: 11309840]

Aoki C, Venkatesan C, Go C, Mong J, Dawson T. Cellular and subcellular localization of NMDA-R1 subunit immunoreactivity in the visual cortex of adult and neonatal rats. J Neurosci 1994;14:5202–5222. [PubMed: 8083731]

Barria A, Malinow R. Subunit-specific NMDA receptor trafficking to synapses. Neuron 2002;35:345–353. [PubMed: 12160751]

Bassand P, Bernard A, Rafiki A, Gayet D, Khrestchatisky M. Differential interaction of the tSXV motifs of the NR1 and NR2A NMDA receptor subunits with PSD-95 and SAP97. Eur J Neurosci 1999;11:2031–2043. [PubMed: 10336672]

Berretta N, Jones RS. Tonic facilitation of glutamate release by presynaptic *N*-methyl-d-aspartate autoreceptors in the entorhinal cortex. Neuroscience 1996;75:339–344. [PubMed: 8931000]

Carroll RC, Zukin RS. NMDA-receptor trafficking and targeting: implications for synaptic transmission and plasticity. Trends Neurosci 2002;25:571. [PubMed: 12392932]

Charton JP, Herkert M, Becker CM, Schroder H. Cellular and subcellular localization of the 2B-subunit of the NMDA receptor in the adult rat telencephalon. Brain Res 1999;816:609–617. [PubMed: 9878886]

Conti F, Barbaresi P, Melone M, Ducati A. Neuronal and glial localization of NR1 and NR2A/B subunits of the NMDA receptor in the human cerebral cortex. Cereb Cortex 1999;9:110–120. [PubMed: 10220224]

DeFelipe J, Conti F, Van Eyck SL, Manzoni T. Demonstration of glutamate-positive axon terminals forming asymmetric synapses in cat neocortex. Brain Res 1988;455:162–165. [PubMed: 3416182]

Dingledine R, Borges K, Bowie D, Traynelis SF. The glutamate receptor ion channels. Pharmacol Rev 1999;51:7–61. [PubMed: 10049997]

Grosshans DR, Clayton DA, Coultrap SJ, Browning MD. LTP leads to rapid surface expression of NMDA but not AMPA receptors in adult rat CA1. Nat Neurosci 2002;5:27–33. [PubMed: 11740502]

Heynen AJ, Quinlan EM, Bae DC, Bear MF. Bidirectional, activity-dependent regulation of glutamate receptors in the adult hippocampus in vivo. Neuron 2000;28:527–536. [PubMed: 11144361]

Kharazia VN, Weinberg RJ. Immunogold localization of AMPA and NMDA receptors in somatic sensory cortex of albino rat. J Comp Neurol 1999;412:292–302. [PubMed: 10441757]

Kind PC, Neumann PE. Plasticity: downstream of glutamate. Trends Neurosci 2001;24:553–555. [PubMed: 11576648]

Lan JY, Skeberdis VA, Jover T, Grooms SY, Lin Y, Araneda RC, Zheng X, Bennett MV, Zukin RS. Protein kinase C modulates NMDA receptor trafficking and gating. Nat Neurosci 2001a;4:382–390. [PubMed: 11276228]

Lan J-Y, Skeberdis VA, Jover T, Zheng X, Bennett MVL, Zukin RS. Activation of metabotropic glutamate receptor 1 accelerates NMDA receptor trafficking. J Neurosci 2001b;21:6058–6068. [PubMed: 11487629]

Liao D, Zhang X, O'Brien R, Ehlers MD, Huganir RL. Regulation of morphological postsynaptic silent synapses in developing hippocampal neurons. Nat Neurosci 1999;2:37–43. [PubMed: 10195178]

Lynch DR, Guttmann RP. Excitotoxicity: perspectives based on *N*-methyl-d-aspartate receptor subtypes. J Pharmacol Exp Ther 2002;300:717–723. [PubMed: 11861773]

Malenka RC, Nicoll RA. Long-term potentiation-a decade of progress? Science 1999;285:1870–1874. [PubMed: 10489359]

Mohrmann R, Kohr G, Hatt H, Sprengel R, Gottmann K. Deletion of the C-terminal domain of the NR2B subunit alters channel properties and synaptic targeting of *N*-methyl-d-aspartate receptors in nascent neocortical synapses. J Neurosci Res 2002;68:265–275. [PubMed: 12111856]

Mori H, Manabe T, Watanabe M, Satoh Y, Suzuki N, Toki S, Nakamura K, Yagi T, Kushiya E, Takahashi T, Inoue Y, Sakimura K, Mishina M. Role of carboxy-terminal region of the GluR epsilon2 subunit in synaptic localization of the NMDA receptor channel. Neuron 1998;21:571–580. [PubMed: 9768843]

Mori H, Mishina M. Structure and function of the NMDA receptor channel. Neuropharmacology 1995;34:1219–1237. [PubMed: 8570021]

Nakanishi S. Molecular diversity of glutamate receptors and implications for brain function. Science 1992;258:597–603. [PubMed: 1329206]

Niethammer M, Kim E, Sheng M. Interaction between the C terminus of NMDA receptor subunits and multiple members of the PSD-95 family of membrane-associated guanylate kinases. J Neurosci 1996;16:2157–2163. [PubMed: 8601796]

Phend KD, Rustioni A, Weinberg RJ. An osmium-free method of epon embedment that preserves both ultrastructure and antigenicity for post-embedding immunocytochemistry. J Histochem Cytochem 1995;43:283–292. [PubMed: 7532656]

Quinlan EM, Philpot BD, Huganir RL, Bear MF. Rapid, experience-dependent expression of synaptic NMDA receptors in visual cortex in vivo. Nat Neurosci 1999;2:352–357. [PubMed: 10204542]

Rao A, Craig AM. Activity regulates the synaptic localization of the NMDA receptor in hippocampal neurons. Neuron 1997;19:801–812. [PubMed: 9354327]

Roche KW, Standley S, McCallum J, Dune Ly C, Ehlers MD, Wenthold RJ. Molecular determinants of NMDA receptor internalization. Nat Neurosci 2001;4:794–802. [PubMed: 11477425]

Sheng M. Molecular organization of the postsynaptic specialization. Proc Natl Acad Sci USA 2001;98:7058–7061. [PubMed: 11416187]

Sheng M, Cummings J, Roldan LA, Jan YN, Jan LY. Changing subunit composition of heteromeric NMDA receptors during development of rat cortex. Nature 1994;368:144–147. [PubMed: 8139656]

Sheng M, Pak DT. Ligand-gated ion channel interactions with cytoskeletal and signaling proteins. Annu Rev Physiol 2000;62:755–778. [PubMed: 10845110]

Steigerwald F, Schulz TW, Schenker LT, Kennedy MB, Seeburg PH, Kohr G. C-Terminal truncation of NR2A subunits impairs synaptic but not extrasynaptic localization of NMDA receptors. J Neurosci 2000;20:4573–4581. [PubMed: 10844027]

Tang SJ, Schuman EM. Protein synthesis in the dendrite. Philos Trans R Soc Lond B Biol Sci 2002;357:521–529. [PubMed: 12028789]

Tang YP, Shimizu E, Dube GR, Rampon C, Kerchner GA, Zhuo M, Liu G, Tsien JZ. Genetic enhancement of learning and memory in mice. Nature 1999;401:63–69. [PubMed: 10485705]

Tovar KR, Westbrook GL. Mobile NMDA receptors at hippocampal synapses. Neuron 2002;34:255–264. [PubMed: 11970867]

Valtschanoff JG, Weinberg RJ. Laminar organization of the NMDA receptor complex within the postsynaptic density. J Neurosci 2001;21:1211–1217. [PubMed: 11160391]

Watanabe M, Inoue Y, Sakimura K, Mishina M. Developmental changes in distribution of NMDA receptor channel subunit mRNAs. Neuroreport 1992;3:1138–1140. [PubMed: 1493227]

Williams JM, Mason-Parker SE, Abraham WC, Tate WP. Biphasic changes in the levels of *N*-methyl-d-aspartate receptor-2 subunits correlate with the induction and persistence of long-term potentiation. Brain Res Mol Brain Res 1998;60:21–27. [PubMed: 9748484]

Woodhall G, Evans DI, Cunningham MO, Jones RS. NR2B-containing NMDA autoreceptors at synapses on entorhinal cortical neurons. J Neurophysiol 2001;86:1644–1651. [PubMed: 11600627]

Yamakura T, Shimoji K. Subunit- and site-specific pharmacology of the NMDA receptor channel. Prog Neurobiol 1999;59:279–298. [PubMed: 10465381]

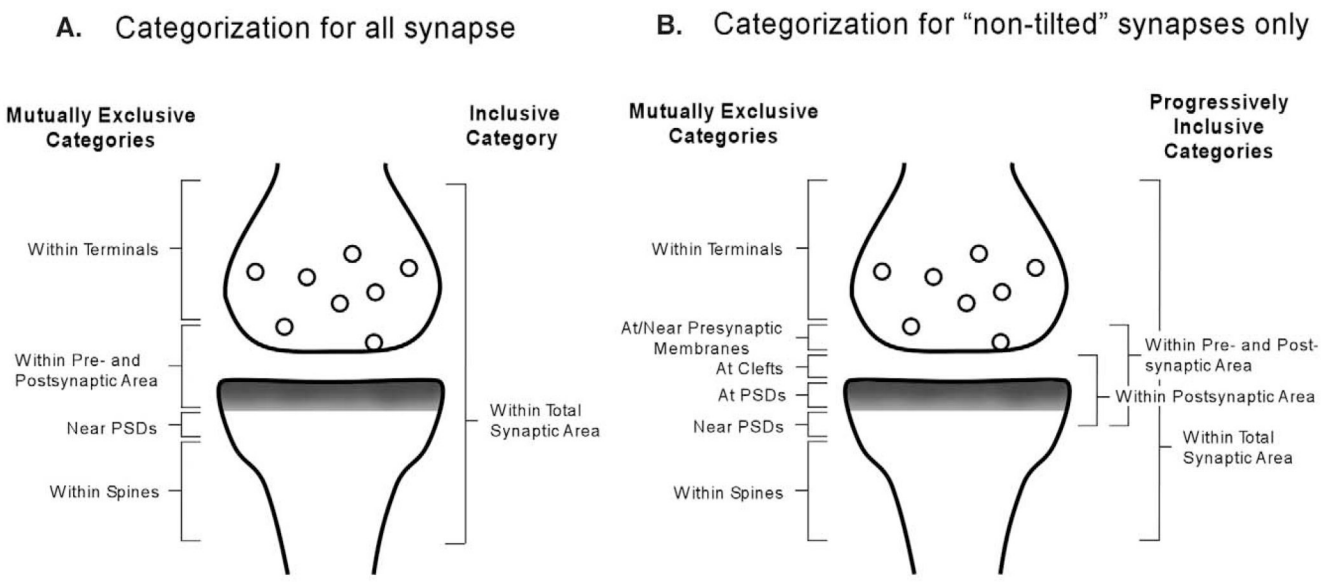

Fig. 1.

(A and B) Schematic drawing of a synaptic profile shows the exclusive and inclusive categories used in the analysis. (A) Categories used to group NR2B immunolabeling in 10 groups of 10 synapses from each hemisphere of each animal. Category "within pre- and postsynaptic area" was used, because this pool contained synapses whose synaptic clefts were not clearly visible. In these synapses, presynaptic and postsynaptic membranes could not be distinguished. (B) For the more selective pool of "non-tilted" synapses only, in which synaptic clefts can be distinctly observed, immunolabeling for NR2B subunit was categorized into one of the mutually exclusive ultrastructural categories, and one or more of the progressively inclusive categories.

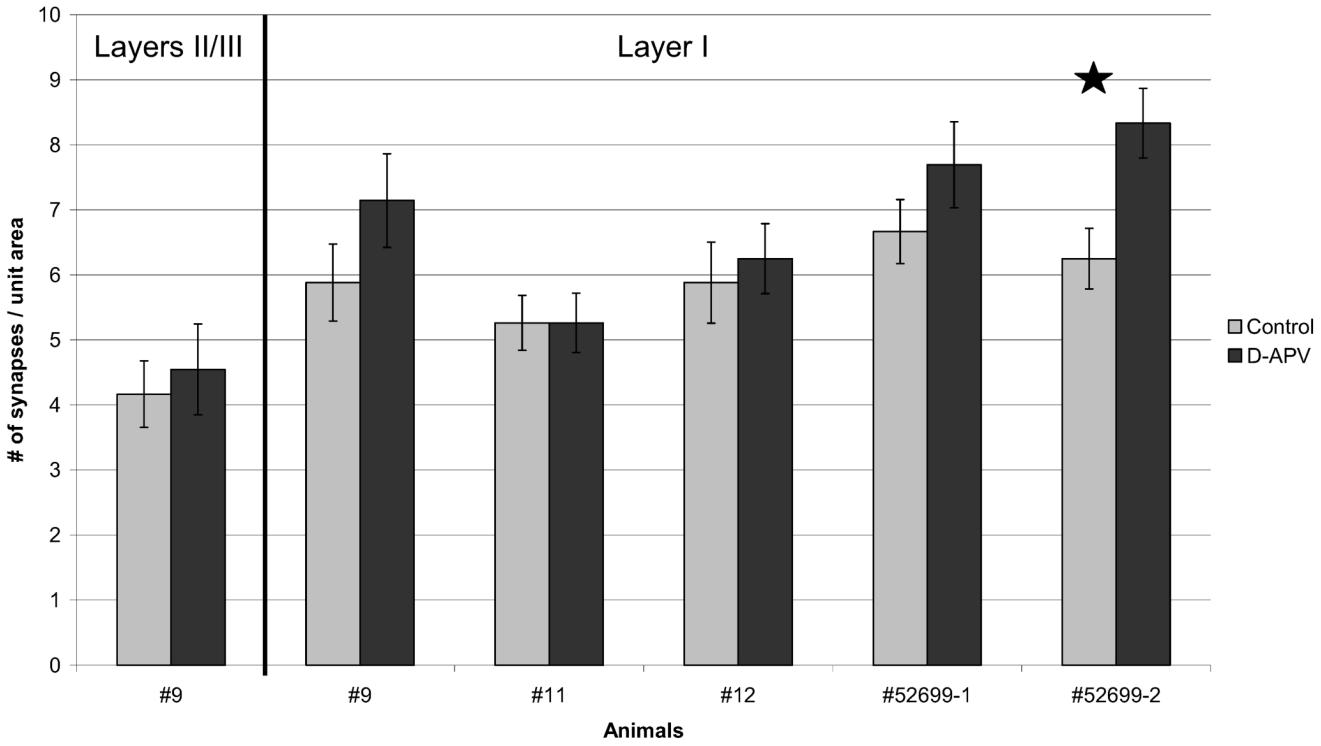

Fig. 2.

D-APV-treatment has minimal effect on synapse density. The number of synapses encountered per unit area (26.60 μm^2 captured in one electron micrograph) was counted for all animals analyzed. Except where noted (first group of bars), tallies are shown for synapses from layer I. In four of the five APV-treated regions, there was a slight increase in synapse density when compared with the contralateral control side. Only in one animal (#52699-2) was this difference significant, as indicated with a star (two-tailed *t*-test; $P<0.05$). Error bars denote S.E.M.

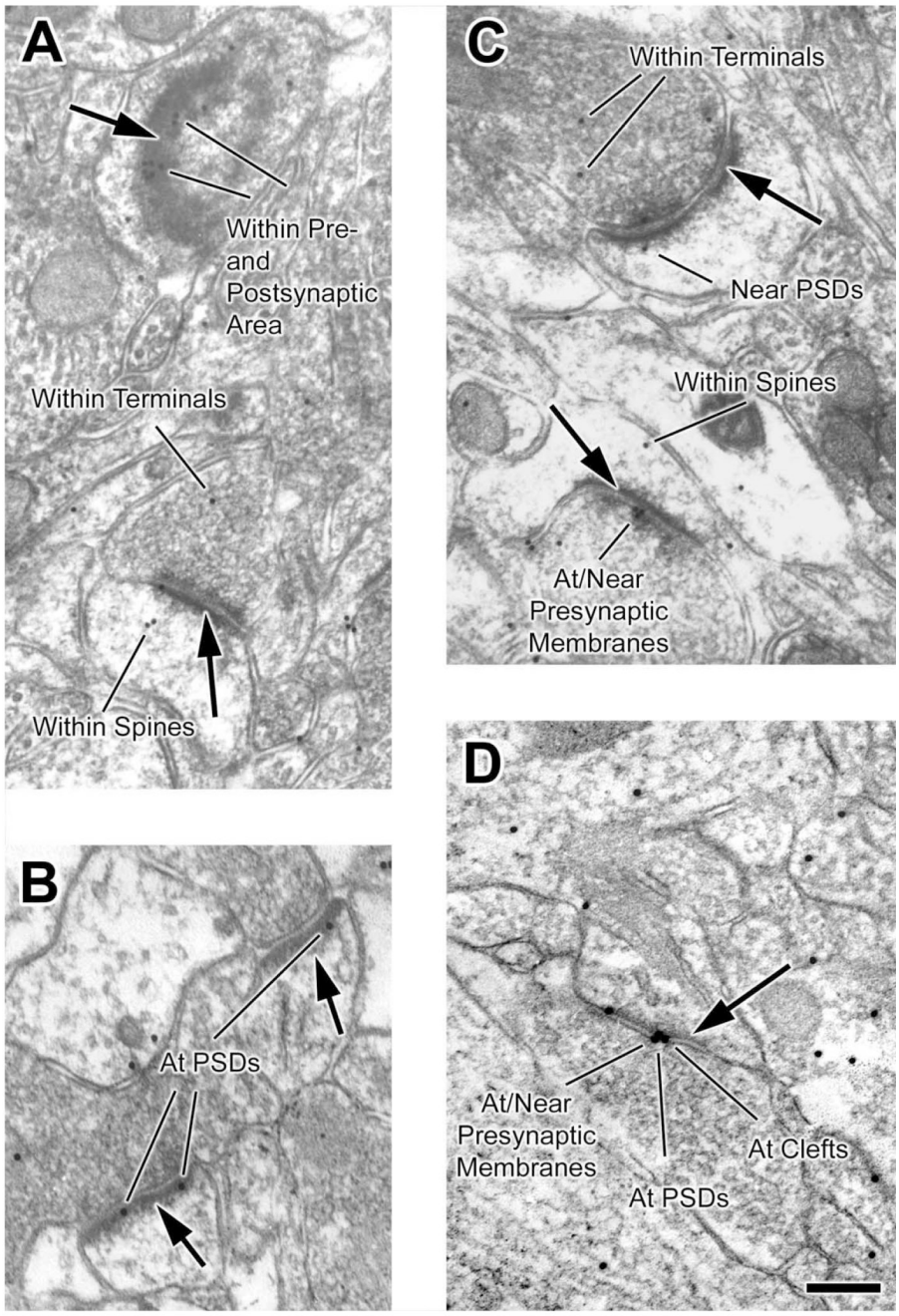

Fig. 3.

Electron microscopy reveals a variety of perisynaptic localizations for NR2B subunits. Images of NR2B-labeled neuropil were taken from layer I of adult somatosensory cortex. Presynaptic terminals are identified by the presence of vesicles. Bold arrows point to postsynaptic densities (PSDs) of spines. The 15 nm gold particles label NR2B subunits. (A) Animal #12, control region. This micrograph captured a tilted, en face plane of PSD (top arrow) along which clusters of gold particles are visible. These gold particles were categorized as “within pre- and postsynaptic area” since we cannot discern whether they are presynaptic or postsynaptic labeling. Synapses such as this top one were eliminated in later analysis that sought to differentiate changes in NR2B immunolabeling in presynaptic and postsynaptic area. (B)

Animal #52699-1, control region. Usually, synapses are observed as profiles with clearly visible synaptic clefts, such as the ones seen in this micrograph. Gold particles “at PSDs” are seen clearly. (C) Animal 12, D-APV region. The “near PSDs” category was defined as comprising those particles residing not on top of a PSD, but within the distance equal to the width of that PSD. NR2B subunit labeling was also found “within spines” and “within terminals” (see panel A for more examples). In addition, particles are present directly above the presynaptic membrane (“at/near presynaptic membranes”). (D) Animal #52699-2, D-APV region. In this micrograph, the spine appears contiguous with the dendritic shaft, contains a prominent spine apparatus, and exhibits a PSD darkening. Particles “at clefts” may be on the presynaptic or postsynaptic side, but for the analysis, labeling “at clefts” (a mutually exclusive category) was included, together with “at PSDs” category, in an inclusive “within postsynaptic area” category. Scale bar=200 nm for all panels.

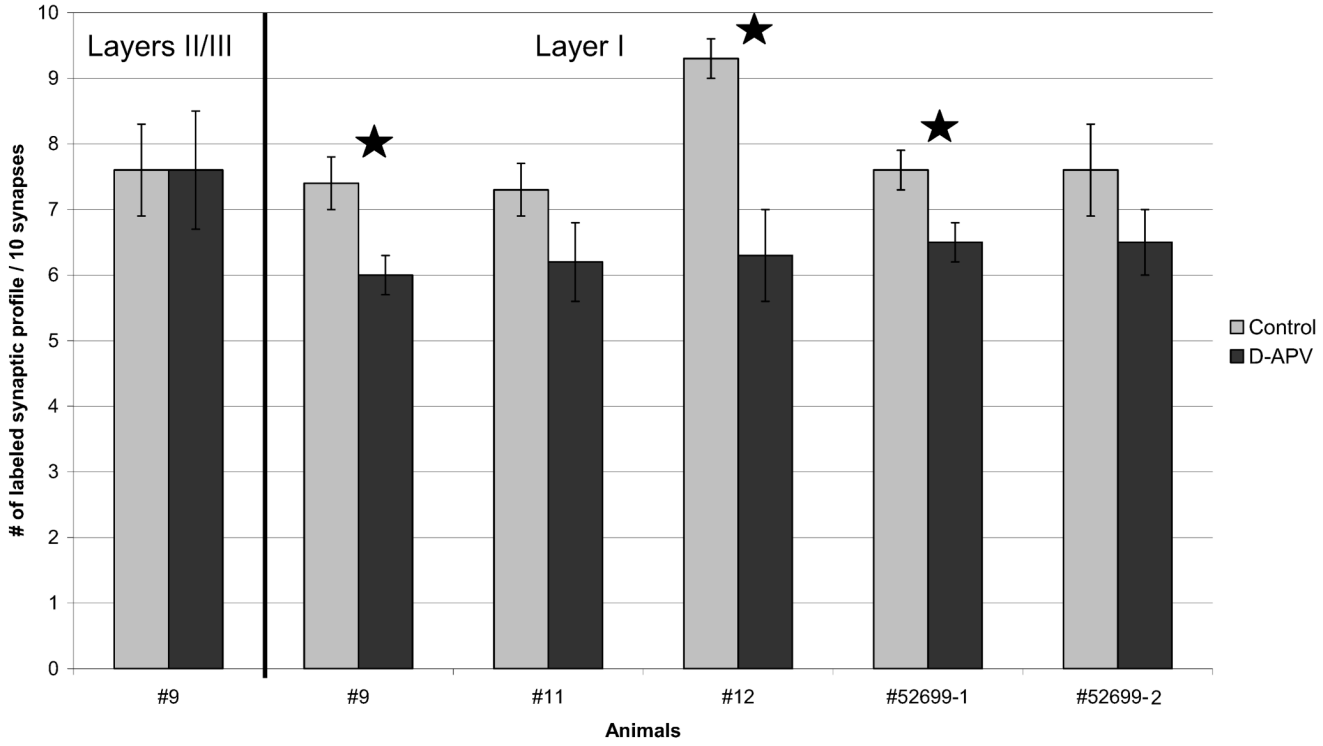

Fig. 4.

APV-treated neuropil exhibits reduction of NR2B-immunoreactive spines and terminals in layer I. For every 10 synapses encountered, the number of synapses with at least one gold particle in the spine and/or the terminal was tallied. Except where noted (first group of bars), tallies are shown for synapses from layer I. Consistently across all animals, there were fewer synapses labeled for NR2B subunits in the D-APV treated neuropil compared with the control tissue from the contralateral hemisphere. In three animals, this reduction in immunoreactive synaptic profiles reached statistical significance, as indicated using stars (two-tailed *t*-test; $P<0.05$). Error bars denote S.E.M. These values are represented in column E of Table 2.

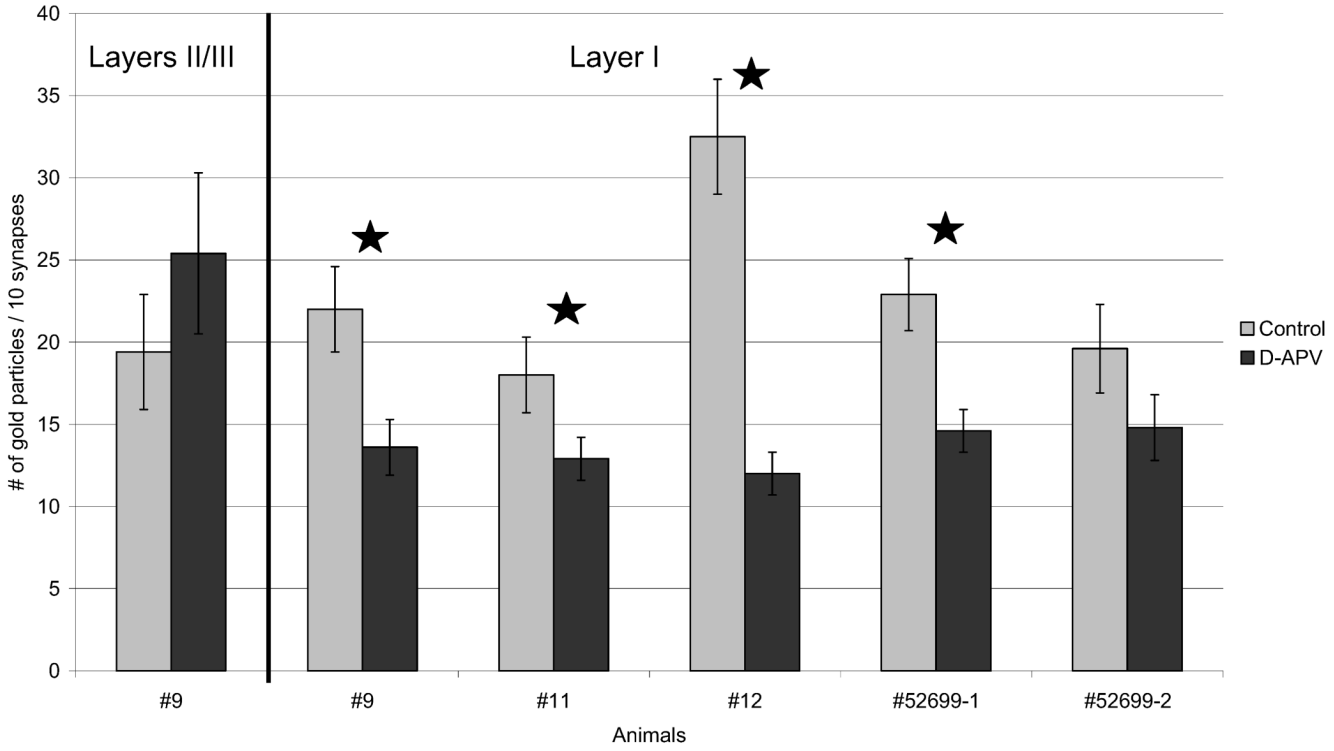

Fig. 5.

APV-treated neuropil shows reduction of NR2B subunit labeling at synapses. For every 10 synapses, the total number of gold particles found in spines and/or terminals was counted. Except where noted (first group of bars), tallies are shown for synapses from layer I. For all five animals, layer I of the drug-treated tissue exhibited a marked reduction in the number of gold particles. The difference was significant in four of the animals, as indicated with a star (two-tailed *t*-test; $P<0.05$). Error bars denote S.E.M. These values are represented in column E of Table 3.

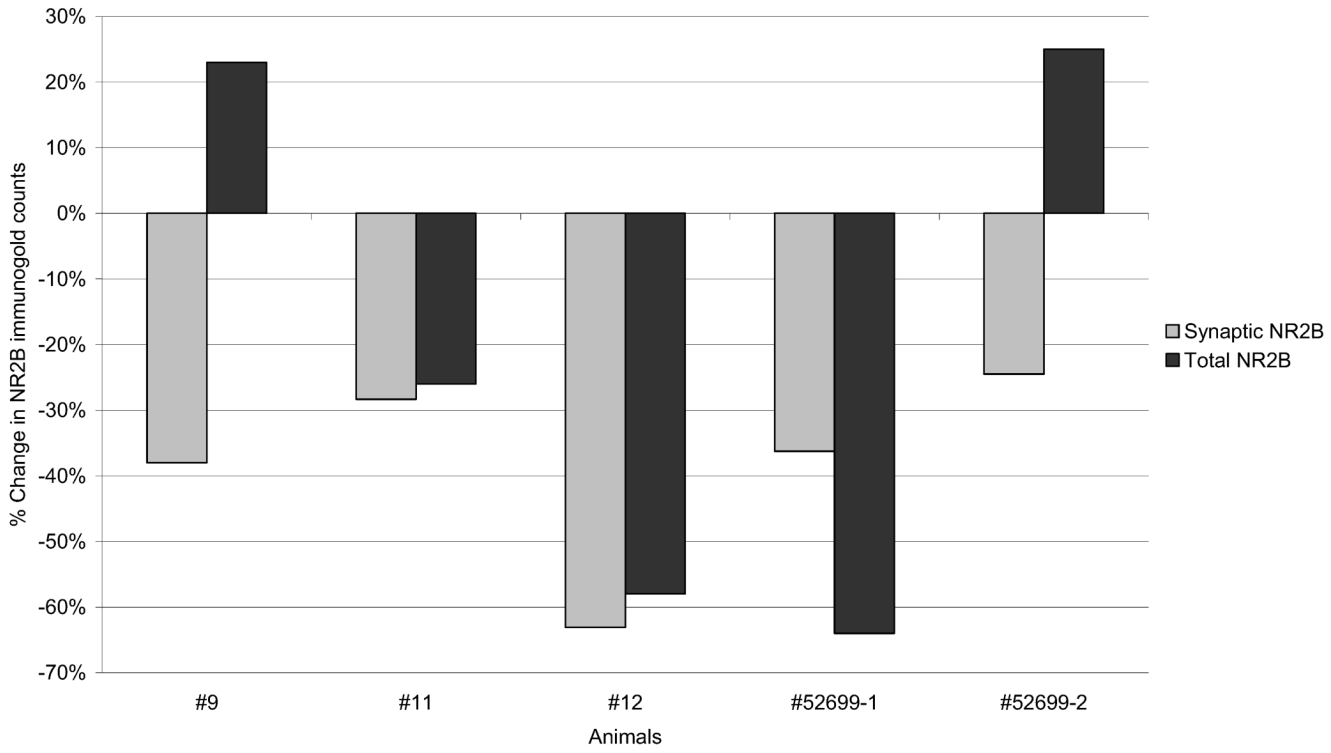

Fig. 6.

Changes in the overall immunoreactivity for NR2B do not always follow the reduction of synaptic NR2B labeling. The percent change in NR2B labeling in layer I after D-APV treatment at synaptic portions only (light gray) and throughout the neuropil (dark gray) are compared. In two animals (#9 and #52699-2), synaptic labeling decreased despite increases in non-synaptic immunoreactivity.

Table 1

Summary of experimental procedures

Animal	Right hemisphere	Left hemisphere	Duration	Embedding material
#9	5mM L-APV	5mM D-APV	30 min	Epon
#10*	5mM D-APV	5mM L-APV	30 min	Epon
#11	5mM L-APV	5mM D-APV	30 min	Epon
#12	5mM D-APV	5mM L-APV	30 min	Epon
#52699-1	Sterile saline	5mM D-APV	1h	Epon-Spurr
#52699-2	Sterile saline	5mM D-APV	2h	Epon-Spurr

* Data from this animal were not analyzed due to respiratory arrest during the surgery.

Table 2

Average number of labeled synapses for groups of 10 synapses (±S.E.M.)[a]

Animal	Drug	No. of groups	A	B	C	D	E
		n	Within terminals	Near PSDs	Within spines	Within pre- and postsynaptic area	Within total synaptic area
#9	L-APV	10	**5.1±0.46**	1.9±0.42	**2.2±0.31**	**4.1±0.46**	**7.4±0.45**
	D-APV	10	**2.7±0.45**	1.4±0.36	**1.2±0.34**	**2.7±0.52**	**6.0±0.35**
#11	L-APV	10	3.8±0.41	1.6±0.39	2.5±0.42	3.8±0.26	7.3±0.39
	D-APV	10	3.1±0.37	1.2±0.52	1.8±0.58	3.2±0.44	6.2±0.58
#12	L-APV	10	**5.3±0.59**	2.8±0.54	**3.4±0.53**	**6.9±0.53**	**9.3±0.27**
	D-APV	10	**2.4±0.53**	1.5±0.48	**1.6±0.32**	**3.7±0.39**	**6.3±0.69**
#52699-1	Saline	10	4.7±0.50	2.1±0.33	2.2±0.47	**4.5±0.53**	**7.6±0.32**
	D-APV	10	4.0±0.47	1.8±0.52	1.6±0.32	**2.9±0.37**	**6.5±0.32**
#52699-2	Saline	10	**4.3±0.45**	1.3±0.32	2.4±0.45	4.4±0.51	7.6±0.72
	D-APV	10	**2.3±0.39**	1.5±0.32	1.4±0.61	3.7±0.62	6.5±0.50

[a]Bold: significant difference between L-APV- and D-APV treated neuropil (two-tailed *t*-test; $P<0.05$).

Table 3

Average number of immunogold particles found in groups of 10 synapses (±S.E.M.)[a]

Animal	Drug	No. of groups	A	B	C	D	E[+]
		n	Within terminals	Near PSDs	Within spines	Within pre- and postsynaptic area	Within total synaptic area
#9	L-APV	10	9.6±1.42	2.2±0.47	**3.6±0.71**	6.5±1.07	**22.0±2.65**
	D-APV	10	6.0±1.66	1.4±0.32	**1.5±0.45**	4.7±1.14	**13.6±1.74**
#11	L-APV	10	6.2±0.84	1.8±0.52	3.7±0.82	6.3±1.12	18.0±2.34
	D-APV	10	4.5±0.59	1.2±0.52	2.1±0.62	5.1±0.82	12.9±1.35
#12	L-APV	10	**11.4±1.38**	**3.4±0.76**	**6.0±1.42**	**11.7±1.44**	**32.5±3.51**
	D-APV	10	**3.3±0.82**	**1.5±0.48**	**2.1±0.48**	**5.1±0.79**	**12.0±1.33**
#52699-1	Saline	10	8.8±1.06	2.8±0.49	4.1±1.14	**7.2±0.91**	**22.9±2.17**
	D-APV	10	6.3±0.88	2.2±0.64	2.4±0.65	**3.7±0.42**	**14.6±1.34**
#52699-2	Saline	10	6.6±0.59	1.9±0.40	4.2±1.51	6.9±1.33	19.6±2.75
	D-APV	10	4.7±0.88	1.9±0.43	2.0±1.01	6.2±1.05	14.8±1.96

[a]Bold: significant difference between L-APV- and D-APV treated neuropil (two-tailed *t*-test; $P<0.05$).

[+]E=A+B+C+D

Table 4

Average number of labeled synapses for groups of 10 “non-tilted” synapses (±S.E.M.)[a]

Animal	Drug	No. of groups	A	B	C	D	E	F	G	H	I
		n	Within terminals	At near Presynaptic membranes	At clefts	At PSDs	Near PSDs	Within spines	Within Postsynaptic area	Within pre- and postsynaptic area	Within total synaptic area
#9	L-APV	7	4.1±0.72	1.7±0.45	1.4±0.46	3.3±0.73	2.0±0.67	**2.4±0.40**	**4.3±0.73**	**5.1±0.44**	**7.6±0.40**
	D-APV	6	2.3±0.67	0.7±0.54	0.3±0.37	1.7±0.37	1.3±0.54	**0.8±0.34**	**2.0±0.40**	**2.5±0.47**	**5.2±0.72**
#11	L-APV	7	3.6±0.22	1.6±0.40	0.4±0.32	1.4±0.40	1.4±0.57	2.6±0.46	1.7±0.51	3.1±0.60	7.0±0.41
	D-APV	5	3.2±0.89	2.0±0.61	0.2±0.22	1.8±0.82	1.2±0.65	1.2±0.82	2.0±0.79	3.2±0.96	5.8±0.82
#12	L-APV	7	**4.9±0.44**	**3.6±0.78**	**2.3±0.61**	**3.0±0.47**	2.6±0.70	3.1±0.44	**4.9±0.72**	**7.1±0.37**	**9.1±0.28**
	D-APV	7	**2.1±0.55**	**1.3±0.39**	**0.9±0.15**	**1.7±0.31**	1.4±0.32	2.0±0.47	**2.1±0.37**	**3.3±0.56**	**6.1±0.80**
#52699-1	Saline	6	4.7±0.46	2.0±0.57	1.7±0.73	1.7±0.37	2.0±0.49	2.3±0.73	2.8±0.87	**4.0±0.89**	7.3±0.73
	D-APV	5	4.6±0.57	2.0±0.71	1.2±0.65	1.6±0.45	2.0±0.61	2.0±0.79	1.0±0.35	**1.8±0.55**	7.0±0.79
#52699-2	Saline	6	3.5±0.79	2.5±0.55	2.5±0.62	2.0±0.63	1.3±0.46	2.7±0.73	4.0±0.75	5.2±0.82	**8.2±0.44**
	D-APV	7	2.1±0.37	1.6±0.46	1.1±0.28	1.3±0.31	1.1±0.28	1.9±0.60	3.3±0.20	4.2±0.45	**6.1±0.44**

[a]Bold: significant difference between L-APV- and D-APV treated neuropil (two-tailed *t*-test; $P<0.05$).

Table 5

Average number of immunogold particles found in groups of 10 “non-tilted” synapses (±S.E.M.)[a]

Animal	Drug	No. of groups	A	B	C	D	E	F	G+	H++	I+++
		n	Within terminals	At/near presynaptic membranes	At clefts	At PSDs	Near PSDs	Within spines	Within postsynaptic area	Within pre- and postsynaptic area	Within total synaptic area
#9	L-APV	7	5.7±1.24	1.9±0.60	**2.3±0.65**	5.1±1.38	2.3±0.65	**3.6±0.66**	7.4±1.65	9.3±1.35	**20.9±2.14**
	D-APV	6	3.7±0.88	0.7±0.54	**0.3±0.23**	4.3±1.67	1.3±0.54	**1.3±0.46**	4.7±1.57	5.3±1.93	**11.7±1.87**
#11	L-APV	7	5.4±0.70	2.3±0.77	0.4±0.32	1.9±0.60	1.7±0.70	**3.4±0.70**	2.3±0.77	4.6±0.97	15.1±1.85
	D-APV	5	4.8±1.19	2.4±0.76	0.2±0.22	2.4±1.20	1.2±0.65	**1.2±0.82**	2.6±1.15	5.0±1.58	12.2±2.51
#12	L-APV	7	**11.0±1.51**	**5.3±1.66**	2.4±0.62	**4.3±0.87**	2.9±0.76	**5.7±1.10**	**6.7±1.07**	**12.0±1.37**	**31.6±4.20**
	D-APV	7	**2.4±0.70**	**1.4±0.52**	1.1±0.28	**1.9±0.60**	1.4±0.32	**2.7±0.61**	**3.0±0.53**	**4.4±0.70**	**11.0±1.45**
#52699-1	Saline	6	8.8±1.48	**2.7±0.67**	3.0±1.39	1.8±0.44	2.7±0.67	4.0±1.79	**4.8±1.53**	**7.5±1.89**	**23.0±3.41**
	D-APV	5	6.4±1.79	**0.8±0.22**	0.6±0.27	0.6±0.45	2.4±0.27	2.2±0.89	**1.2±0.55**	**2.0±0.71**	**13.0±2.09**
#52699-2	Saline	6	5.5±1.16	2.4±0.55	2.8±0.77	3.2±1.15	1.7±0.54	4.8±2.05	6.0±1.47	8.5±1.89	20.5±4.43
	D-APV	7	4.7±0.65	1.9±0.55	1.4±0.40	1.9±0.60	1.6±0.32	2.4±0.91	4.9±0.68	6.7±0.90	13.9±1.92

[a] Bold: significant difference between L-APV- and D-APV treated neuropil (two-tailed *t*-test; $P<0.05$).

[+] G = C+D.

[++] H = B + C + D.

[+++] I=A+E + F + H.